

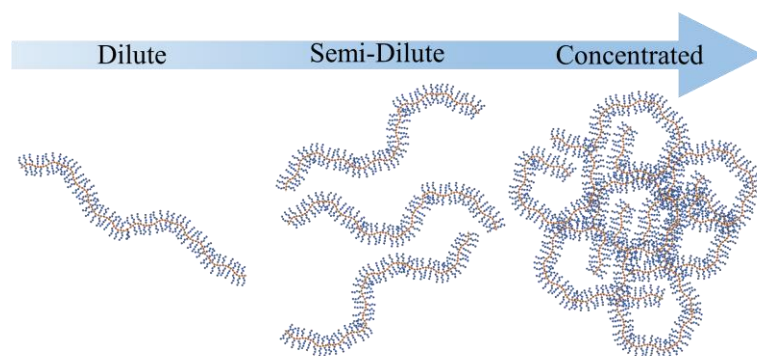
# The Concentration Dependence of the Size and Symmetry of a Bottlebrush Polymer in a Good Solvent

Daniel F. Sunday<sup>1\*</sup>, Alexandros Chremos,<sup>1\*</sup> Tyler B. Martin<sup>1</sup>, Alice B. Chang<sup>2</sup>, Adam B. Burns<sup>1</sup>, Robert H. Grubbs<sup>2</sup>

1. Materials Science and Engineering Division, National Institute of Standards and Technology, Gaithersburg, MD 20899, United States
2. Division of Chemistry and Chemical Engineering, California Institute of Technology, Pasadena, CA 91125, United States

Email: \* [Daniel.Sunday@nist.gov](mailto:Daniel.Sunday@nist.gov), \* [Alexandros.Chremos@nist.gov](mailto:Alexandros.Chremos@nist.gov)

## TOC Graphic



## Abstract

Bottlebrush polymers consist of a linear backbone with densely grafted side chains which impact the rigidity of the molecule. The persistence length of the bottlebrush backbone in solution is influenced by both the intrinsic structure of the polymer and by the local environment, such as the solvent quality and concentration. Increasing the concentration reduces the overall size of the molecule due to the reduction in backbone stiffness. In this study we map out the size of a bottlebrush polymer as a function of concentration for a single backbone length. Small-angle neutron scattering (SANS) measurements are conducted on a polynorbornene-based bottlebrush with polystyrene side chains in a good solvent. The data are fit using a model which provides both the long and short axis radius of gyration ( $R_{g,2}$  and  $R_{g,1}$ , respectively), providing a measure for how the conformation changes as a function of concentration. At low concentrations a highly anisotropic structure is observed ( $R_{g,2}/R_{g,1} \approx 4$ ), becoming more isotropic at higher concentrations ( $R_{g,2}/R_{g,1}$

$\approx 1.5$ ). The concentration scaling for both  $R_{g,2}$  and the overall  $R_g$  are evaluated and compared with predictions in the literature. Coarse-grained molecular dynamics simulations were also conducted to probe the impact of concentration on bottlebrush conformation showing qualitative agreement with the experimental results.

## Introduction

Bottlebrush and comb polymers are a class of branched macromolecules consisting of a linear backbone and side chains which alter the intrinsic stiffness of the backbone.<sup>1</sup> The coalescence of a variety of synthetic approaches has resulted in straightforward fabrication of bottlebrushes with wide ranging chemistries and high tunable structure, thereby enabling customization of material properties.<sup>2-6</sup> These materials have potential applications in photonics,<sup>7,8</sup> as pressure sensitive adhesives<sup>9,10</sup> and in the biomedical space.<sup>6,11</sup> This wide suite of potential applications has prompted a significant interest in understanding the relationship between key molecular parameters – such as the backbone degree of polymerization ( $N_B$ ), side chain degree of polymerization ( $N_S$ ), and grafting density ( $z$ ) – and the resulting conformation both in solution and the melt.<sup>12-17</sup> In addition to the aforementioned parameters, the conformations of bottlebrush polymers are highly sensitive to concentration.<sup>18-20</sup> Previous reports have applied scaling analyses to predict the relationships between structure and conformation as a function of concentration.<sup>21-23</sup> In this work we will use both experiment and simulations to examine the detailed changes in the conformation of a bottlebrush polymer over concentrations spanning the dilute limit to a concentrated solution.

The conformational properties of bottlebrush polymers in solution are often studied by a combination of light scattering and small-angle neutron scattering (SANS). The shape of the polymer can be described by the radius of gyration ( $R_g$ ), which can be broken down into a long and short axis to detail structural asymmetry in the material (shown in Figure 1). Trends in the various metrics of molecular shape have been reported in recent studies in solution<sup>14,24</sup> and in melt<sup>13,25</sup> where a crossover from a spherical/ellipsoidal-like molecular shape (equivalent to star polymers) when the backbone is short relative

to side chains to highly anisotropic molecular shape when the backbone becomes much longer compared to the side chain length is observed. This crossover is, however, not trivial as the molecular shape of bottlebrush polymers initially tends to become more spherical with increasing the backbone length until a critical threshold is reached and bottlebrush polymers become more anisotropic.

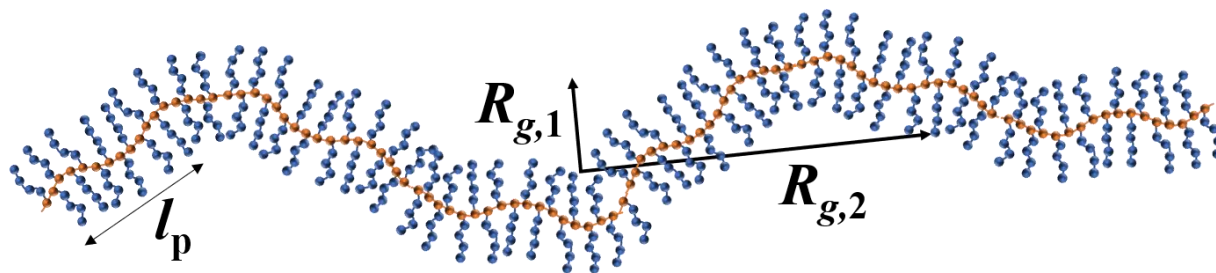


Figure 1: Schematic of the bottlebrush structure at low concentrations. The solution shape can be characterized by a long ( $R_{g,2}$ ) and short axis ( $R_{g,1}$ ). The rigidity of the backbone is quantified through the persistence length ( $l_p$ ).

Beyond  $R_g$ , the structure of a bottlebrush polymer is often described by the persistence length ( $l_p$ ) of the backbone, which describes the rigidity of the system and is known to be a function of the side chain length, chemistry, solvent quality, and the local environment.<sup>16,26</sup> The experimentally determined  $l_p$  is by necessity presented as a single value, but in reality  $l_p$  is a function of position along the chain. In linear polymers, the end groups are more flexible relative to the core, which results in  $l_p$  changing continuously as a function of chain position. This effect is amplified in bottlebrushes compared to linear chains as the confinement of the side chains is greatly alleviated near the chain ends. As a result, as the side chain length increases, the dependence of  $l_p$  on position along the backbone becomes stronger.<sup>12,27</sup> This dependence on backbone length should be considered when comparing values for  $l_p$  across different materials, and going forward in this document the discussion will center on the average  $l_p$  unless otherwise noted. Indeed, simulation studies on the conformational properties of isolated bottlebrush polymers under athermal solvent conditions have revealed that for a well-defined persistence length to be extracted at the asymptotic limit,

where the bottlebrush satisfies the self-avoiding walk statistics, requires large molecular masses for the bottlebrushes.<sup>27,28</sup> The contributions of the side chains to  $l_p$  can be represented by Equation 1, which separately considers the intrinsic persistence length of the backbone ( $l_{po}$ ) in the first term and the contributions from the side chains in the second term ( $N_s$  is the degree of polymerization of the sidechains,  $k$  is the scaling prefactor and  $n$  is the scaling exponent). The value of  $n$  will be a function of the solvent quality, grafting density, and backbone length. This also assumes that the system is sufficiently dilute such that the persistence length is independent of concentration. Unperturbed melt scaling analysis predicts  $n = 1.375$ ;<sup>22</sup> when excluded volume effects are included for both the backbone and side chains,  $n = 1.875$ .<sup>1</sup> Previously reported measurements on a series of bottlebrushes with a poly(methacrylate) (PMA) backbone, polystyrene (PS) side chains, and varied side chain lengths in either d-toluene (a good solvent) or d-cyclohexane (a near-theta solvent) produced values of  $n$  which were very close to the theoretical predictions,  $n = 1.42$  (cyclohexane) and  $n = 1.79$  (toluene). (These predictions assume a fully grafted chain with flexible side chains.)<sup>16</sup> These measurements were conducted on polymers with long backbones ( $N_B > 1000$ ) such that backbone length effects on  $l_p$  were likely small.

$$l_p = l_{po} + kN_s^n \quad (1)$$

Compared to the vinyl class, the norbornene-based bottlebrushes have been reported more recently, and fewer investigations have been performed into their solution structure.<sup>14,24,29-31</sup> The primary difference between norbornene-based bottlebrushes and vinyl-based bottlebrushes is that for fully grafted vinyl systems have one side chain for every two backbone carbons, while fully grafted norbornene systems have one side chain for every five backbone carbons. This intrinsically limits the grafting density of the norbornene chemistry, unless there are multiple branches from each backbone monomer.<sup>32</sup> Studies on the norbornene-based bottlebrushes have been largely unable to extract clear scaling relationships, possibly due to concentration effects, as most measurements were carried out at  $\approx 1$  wt %. As will be shown later in this document, this is clearly in a region where concentration can have a significant effect on polymer conformation, even for backbones with moderate length.

The impact of solution volume fraction ( $\phi$ ) on polymer conformation is well understood for simpler architectures. For linear polymers,  $R_g$  is independent of concentration in the dilute regime until the overlap concentration is reached, at which point  $R_g$  scales with  $\phi^{-1/8}$ . Star polymers also show a transition from a concentration independent regime to a semi-dilute regime where  $R_g \sim \phi^{-1/8}$ .<sup>33</sup> Stronger dependencies on  $\phi$  have been predicted at higher concentrations, up to  $R_g \sim \phi^{-3/4}$  for star polymers,<sup>34</sup> but to the best of our knowledge have not been observed experimentally. Several reports on bottlebrushes have begun to explore their concentration dependence. Small-angle neutron scattering (SANS) measurements on bottlebrushes composed of poly(2-hydroxyethyl methacrylate) (PHEMA) backbones and poly(*t*-butyl acrylate) (PTBA) side chains ( $N_B \approx 1600$ ,  $N_S = 61$ ,  $z = 0.5$ ) show a reduction in the persistence length from 17.5 nm at infinite dilution to 5 nm at a volume fraction of 0.038, with a corresponding reduction in  $R_g$ .<sup>18</sup> The PHEMA-*g*-PTBA samples exhibited a dilute, concentration-independent regime, followed by a semi-dilute region where  $R_g \sim \phi^{-1/8}$ , and finally a third region where  $R_g \sim \phi^{-17/56}$ , although the limited number of data points makes exact extraction of the scaling regimes difficult. The first scaling analysis performed by Borisov et al. on these systems predicted four separate concentration scaling regimes for the polymer end-end distance ( $R_e$ ).<sup>23</sup> For bottlebrush polymers in a good solvent there is initially a dilute concentration independent regime before increasing concentration results in semi-dilute regime where  $R_e \sim \phi^{-1/8}$ . While it is generally straightforward to estimate the overlap concentration for a flexible polymer or a fully rigid rod the accurate prediction of the overlap concentration for a semiflexible polymer is more challenging.<sup>35</sup> For a rigid rod the overlap concentration is proportional to  $M/(N_a L^3)$ , where  $M$  is the molecular mass,  $N_a$  is avogadro's number and  $L$  is the rod length. For a semiflexible chain the overlap concentration is proportional to  $M/(N_a L^{*3})$  where  $L^* = (l_p L)^{1/2}$ . At higher concentrations the exponent initially increases,  $R_e \sim \phi^{-17/56}$ , before moving to the highest concentration regime where  $R_e \sim \phi^{-1/8}$ . A detailed scaling analysis was recently performed by Paturej and co-workers which predicted four scaling regimes based on the length scales at which excluded volume interactions were screened.<sup>21</sup> In the first regime beyond the dilute (concentration-independent) region, the excluded volume effects are screened on a length scale commensurate with the contour length, resulting in  $R_e \sim \phi^{-1/8}$ , identical to a linear chain under those conditions. At higher concentrations, the

interactions are screened at length scales on the order of the persistence length and  $R_e \sim \phi^{-1/4}$ . At the highest concentrations they predict that screening of the inter side chain and intra side chain excluded volume leads to  $R_e \sim \phi^{-4/13}$  and  $R_e \sim \phi^{-2/5}$ . Corresponding predictions were also made for the scaling of  $l_p$  with  $\phi$ .

There are three general approaches used to model the scattering data from the bottlebrush architecture, (1) size only, which utilizes a material-agnostic approach such as the generalized Guinier-Porod (GGP) model to extract length scales and power law slopes,<sup>29,36,37</sup> (2) the wormlike chain model<sup>14,16,20</sup> and (3) comparison with the Fourier transform of molecular conformations calculated from simulations.<sup>12,38</sup> While utilizing well benchmarked atomistic simulations would be the most robust approach to fitting the data, the large size of the bottlebrush makes this computationally prohibitive, although efforts are underway to tackle those issues.<sup>39</sup> Our recent work discussed some of the challenges inherent in using the flexible cylinder model, showing that while it provides direct access to a value for  $l_p$ , the correlations between parameters and multimodality of the goodness of fit space makes utilization of that model challenging.<sup>37</sup> The GGP model provides a robust alternative with direct access to both the long and short axis  $R_g$ , making it well suited for general characterization of asymmetric structures in solution. An estimate of  $l_p$  can then be extracted from  $R_{g,2}$  using Equation 2 ( $L_c$  is the contour length of the backbone based on  $N_{BB}$ ).<sup>40</sup>

$$R_{g,2} = \left( \frac{L_c l_p}{3} - l_p^2 + \frac{2l_p^3}{L_c} - 2[1 - e^{-L_c/l_p}] \frac{l_p^4}{L_c^2} \right)^{1/2} \quad (2)$$

Coarse grained molecular dynamics simulations play a useful role in guiding the understanding of structure-conformation relationships in bottlebrush systems but provide limited access to the relevant length and time scales for these systems. This problem is particularly acute for polymers in solution when the time scales of interest are longer than that of the solvent dynamics, where the majority of the computational resources are spent in the description of the solvent particles. Implicit solvent models, where the solvent is replaced by an effective interaction between the polymer segments, provides significant savings in computational time. Thus, it is not surprising that many computational studies of polymers<sup>41,42</sup> and in particularly bottlebrush polymers in solution<sup>12,20,21,24</sup> frequently rely on implicit solvent polymer models.

However, a sole reliance on implicit solvent models could lead to erroneous conclusions as various solvent effects not incorporated into the model may play an important role into the phenomenon of interest. Indeed, implicit solvent models rely on a higher level of coarse-grained description of the system of interest that could mean that important structural and dynamical information may be lost in the process of coarse-graining.<sup>43,44</sup> Here, we utilize an explicit solvent model for bottlebrush polymers at different concentrations and we find that our model captures the trends in the molecular conformational changes found in the experiments.

## Materials and Methods

**Sample Preparation:** Bottlebrush polymers were prepared by the grafting-through ring-opening metathesis polymerization (ROMP) of polystyrene (PS) macromonomers. The molecular weight and dispersity were characterized using size-exclusion chromatography. Additional details are provided elsewhere.<sup>45</sup> This report focuses on the bottlebrush PNB<sub>105-g100</sub>-PS<sub>40</sub>, for which a polynorbornene backbone ( $N_B = 105$ ) bore pendant polystyrene side chains ( $N_S = 40$ ) at 100% grafting density ( $z = 1$ ). The dispersity for the brush was  $\mathcal{D} = 1.03$ .

**Small-angle neutron scattering (SANS):** PNB<sub>105-g100</sub>-PS<sub>40</sub> was dissolved in d8-toluene, a good solvent for PS, at a volume fraction of 0.086. SANS measurements were conducted on the 10 m SANS line at the National Center for Neutron Research (NCNR). Following the measurement, the sample was diluted with additional d8-toluene and the measurement was repeated. The data were corrected for detector sensitivity, empty beam scattering, and sample thickness and transmittance and plotted as absolute intensity versus the magnitude of the momentum transfer vector  $q = (4\pi/\lambda) \sin \theta$ , where  $2\theta$  is the scattering angle. The data were fit using both the GGP model and the flexible cylinder model, both of which were implemented in SASView.<sup>46</sup> Optimizations were conducted utilizing the directed evolution Monte-Carlo (DREAM) algorithm, which samples the parameter space based on the relative goodness of fit, providing direct access to parameter distributions and uncertainties. Reported uncertainties represent the 95% confidence intervals for the sampled populations.<sup>47</sup>

## Simulation methods

Our system consists of bottlebrush polymers in explicit solution; there are  $N_p$  polymers in the simulation box. A bottlebrush polymer has two main features, namely a backbone and side chains. The backbone is composed of  $N_b$  segments and the side chains each is composed of  $M$  segments. Each bottlebrush polymer has  $f$  side chains, where one end is grafted along the backbone in a uniform fashion. Thus, the total number of interaction centers per bottlebrush polymer is  $M_w = fM + N_b$ . The main focus of the current study is on the following set of molecular parameters: side chain length  $M = 10$  segments, backbone length  $N_b = 40$  segments, and grafting density  $f/N_b = 1$  corresponding to one side chain per backbone segment. The overall molecular mass of the bottlebrush polymer is  $M_w = 440$ . Developing exact translations between coarse grained simulations and experiments is an ongoing challenge, therefore these parameters were chosen to reflect the approximate structure of the experimentally studied molecule.

The interactions between all types of segments are described by the cut-and-shifted Lennard-Jones (LJ) potential where  $\epsilon$  and  $\sigma$  define the units of energy and length and set equal to unity, unless stated otherwise. In explicit solvent simulations, the solvent is represented by single LJ-particles and all the interactions (segment-segment, solvent-solvent, and segment-solvent) are described by a cutoff distance  $r_c = 2.5 \sigma$ . The total number of interaction centers in explicit solvent simulations was  $N = 252\,000$ . We set the segment-solvent interaction  $\epsilon_{\text{sol-seg}} / \epsilon = 1.2$ , corresponding to a Flory-Huggins parameter  $\chi \approx -3.3$ , which represents a good solvent.<sup>48</sup> The segments along a chain are connected with their neighbors via a stiff harmonic spring,  $V_H(r) = k(r - l_0)$ , where  $l_0 = 0.99 \sigma$  is the equilibrium length of the spring and  $k = 2500 \epsilon/\sigma$  is the spring constant. In terms of the units of real polymer chains, the beads should be identified with statistical segments of a flexible polymer having a typical scale of 1 nm to 2 nm.

Simulations were performed in a cubic box with length  $L$ ; periodic boundary conditions were applied in all three directions. We utilized the large-scale atomic/molecular massively parallel simulator (LAMMPS).<sup>49</sup> Simulations were performed in the  $NVT$  ensemble after equilibration in the  $NPT$  ensemble at the desired temperature. Time-averaging was conducted for  $O(10^8)$  time steps after equilibration. The

time step was set to  $\delta t = 0.005 \tau$ , where  $\tau = \sigma (m / \epsilon)^{1/2}$  is the unit of time, where  $m$  is the unit of mass. Temperature and pressure are measured in units of  $\epsilon / k_B$  and  $\sigma / \epsilon$ , respectively. Simulations were performed at temperature  $T = 0.8$ , and  $\langle P \rangle \approx 0.1$  in reduced units; these conditions correspond to a temperature well above the glass transition temperature in the liquid state near atmospheric pressure.

## Results and Discussion

In order to study how concentration changes the solution structure of a bottlebrush in a good solvent PNB<sub>105-g100</sub>-PS<sub>40</sub> was dissolved in d8-toluene and then sequentially diluted, SANS measurements were conducted at each dilution. The results of these measurements are shown in Figure 2. At  $\phi = 0.004$ , the measurement results in a scattering curve with a plateau at low  $q$ , followed by regions with two distinct power law slopes,  $q \approx 0.01\text{--}0.035 \text{ \AA}^{-1}$  and  $q \approx 0.035\text{--}0.07 \text{ \AA}^{-1}$ . A third power law region exists for  $q \geq 0.09 \text{ \AA}^{-1}$ , but at low concentrations it is difficult to distinguish this from the background. The lowest concentrations measured ( $\phi = 0.002$  and  $0.0009$ ) do not appear to contain the two distinct scaling regions prior to approaching the background but it is difficult to determine if this is because of a structural shift or due to the overall reduction in scattering intensity. As the concentration increases, the curve gradually shifts to higher  $q$ , indicating that the overall size of the structure decreases. At  $\phi \geq 0.0542$  there is a clear shift in the scattering where a structure factor emerges and the concentration dependence of the shape of scattered intensity is diminished. This also coincides with the disappearance of the two power law slopes and emergence of a single decay below  $q = 0.1 \text{ \AA}^{-1}$ .

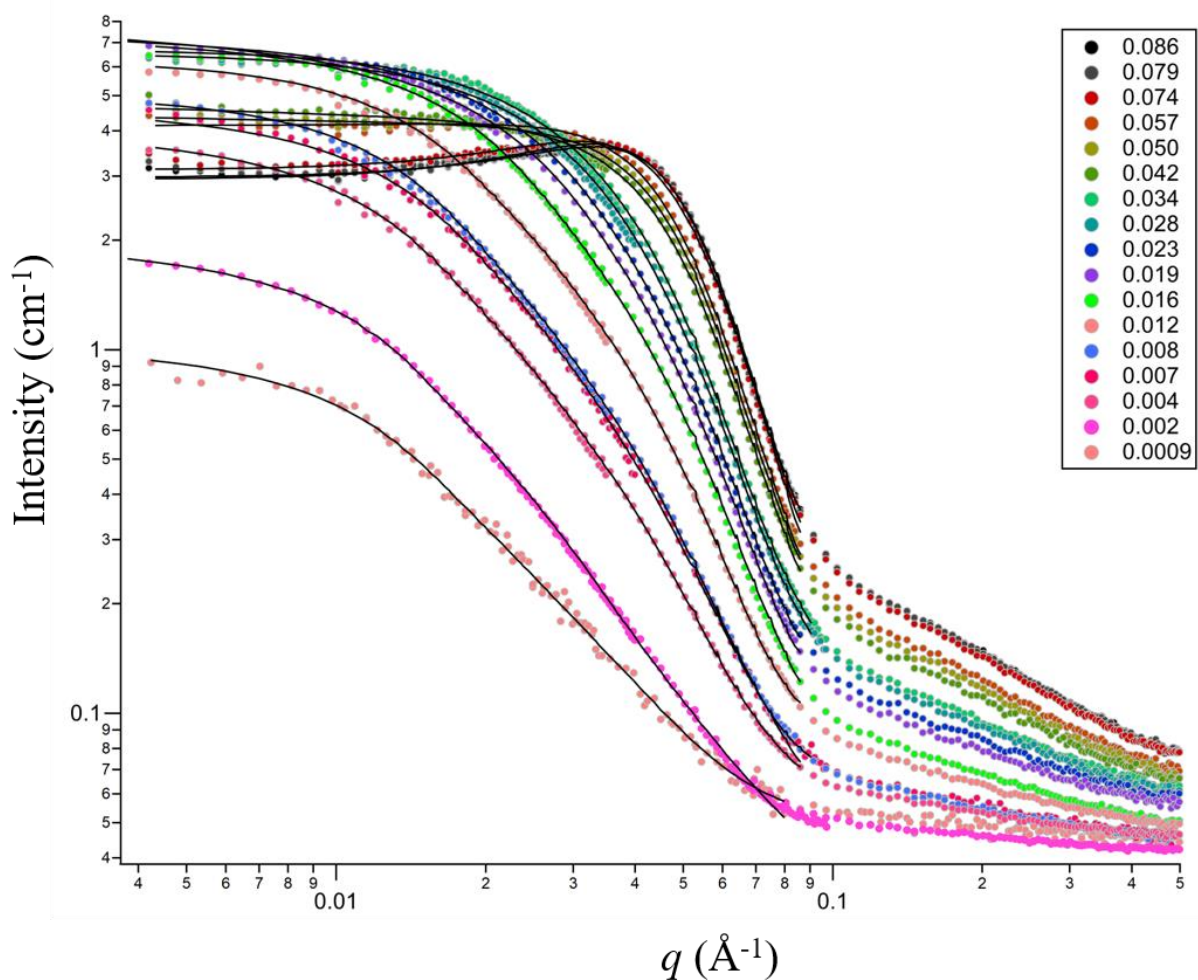


Figure 2: Results of SANS measurements on  $\text{PNB}_{105}\text{-}g\text{-PS}_{40}$  as a function of concentration ranging from  $\phi = 0.0009$ – $0.086$  in d8-toluene, a good solvent. A structure factor emerges in the scattering at  $\phi \geq 0.042$ . Experimental data is shown in colored circles, and the experimental fits to the data using the generalized Guinier-Porod model are shown as solid lines.

The scattering data were analyzed with the GGP model (described in detail in the supplemental information [SI]) which is a structure agnostic model which utilizes a shape factor ( $s$ ) to account for the dimensionality ( $d$ ) of the scattering object ( $d=3-s$ ).<sup>36</sup> The two layer model allows for the determination of both the  $R_g$  of the long axis ( $R_{g,2}$ ) and the short axis ( $R_{g,1}$ ). The results of these fits are shown in Figure 3A as a function of the polymer volume fraction. At the lowest volume fraction ( $\phi = 0.0009$ ),  $R_{g,2}$  was found to be  $99.4 \pm 3.9 \text{ \AA}$  and  $R_{g,1}$  was  $22.5 \pm 1.3 \text{ \AA}$  ( $R_{g,2}/R_{g,1} = 4.42 \pm 0.18$ ), consistent with the idea that a bottlebrush of sufficient backbone length will form an anisotropic shape in a good solvent. In addition to  $R_g$ , the GGP

uses a shape parameter to describe the mass scaling in each length scale regime. A rod ( $d = 2$ ) has a shape parameter of 1 and a perfect sphere ( $d = 3$ ) will have a shape parameter of 0, while Gaussian and swollen polymer coils are described by  $s = 2$  and  $5/3$ , respectively. The shape parameter corresponding to the larger length scale feature,  $s_2$ , was found to be  $1.37 \pm 0.06$  at  $\phi = 0.0009$ , consistent with an elongated cylindrical shape. The shape parameter corresponding to the smaller length scale feature ( $s_1$ ) was less than 0.1 for all concentrations, indicating that the  $q$  range is sufficient to capture the length scale of the whole molecule. The overall  $R_g$  can be estimated from  $R_{g,2}$  and  $R_{g,1}$  assuming that an ellipsoid captures the average shape of the molecule in solution, this scaling is included in Figure 3A

Increasing concentration is known to decrease the size of branched macromolecules through a reduction in excluded volume effects, and this behavior is observed here where as the solution concentration increases both  $R_g$  and  $R_{g,2}$  decrease. The log-log plot in Figure 3A illustrates the emergence of four distinct scaling regimes: (I)  $\phi < 0.0015$  the dilute regime where the size of the molecule is concentration independent, (II)  $0.0015 < \phi < 0.012$  the semi-dilute regime where  $R_g \sim \phi^{-0.11}$  and  $R_{g,2} \sim \phi^{-0.12}$  (III)  $0.012 < \phi < 0.032$  a semi-concentrated regime where  $R_g \sim \phi^{-0.35}$  and  $R_{g,2} \approx \phi^{-0.58}$ , and (IV)  $0.04 < \phi$  the concentrated regime where  $R_g \sim \phi^{-0.10}$  and  $R_{g,2} \sim \phi^{-0.15}$ . In comparing these observed scaling results to predicted values it is important to note that the scaling predictions provide values for  $R_e$ , rather than  $R_g$ . For linear polymers the scaling behavior for the two values will be identical, but it is not clear whether this will hold for rigid polymers. The observed values in the semi-dilute regime (II) for both  $R_g$  and  $R_{g,2}$  are close to  $R_g \approx \phi^{-1/8}$ , in good agreement with previous solution scattering measurements of linear, star and bottlebrush polymers in the semi-dilute region. This suggests a universal concentration dependence for polymers in solution at low concentrations, regardless of architecture. While the uncertainty is higher for the lowest concentration measured due to the reduced intensity and scatter in the data, it appears that the value for  $R_{g,2}$  falls below value anticipated by the scaling trend, indicating that below this concentration the structure will be independent of concentration and can be classified as dilute (I). Upon transitioning from the semi-dilute regime to the semi-concentrated regime (III), the observed scaling exponents for the overall  $R_g$  and the long

axis diverge, with  $R_{g,2} (\phi^{-0.58})$  having a stronger concentration dependence than the overall  $R_g (\phi^{-0.35})$ . The structure becomes noticeably more symmetric as it moves through this region, with the short axis  $R_{g,1}$  increasing slightly and a corresponding reduction in  $s_1$  as  $R_{g,2}/R_{g,1}$  approaches 1. The measured scaling exponent for  $R_g$  falls between the predicted exponent for the third and fourth regime predicted by Paturej and Kreer. They predict  $R_e \approx \phi^{-4/13}$  when screening occurs between interpenetrating sidechains of different molecules in their third concentration regime and  $R_e \approx \phi^{-2/5}$  when screening of the free volume for sidechains on the same molecule. This may imply that those two regions are not distinct, but that the screening occurs simultaneously between inter- and intra-molecular sidechains. It is also possible that other affects, such as backbone-solvent interactions, which are still poorly understood, contribute to the size scaling in this region. The second regime they predict, scaling on the order of the persistence length, is either absent or occurs over such a small volume fraction region as to be unobservable in the experimental data. At the highest concentrations measured in this work, a fourth regime is encountered, coinciding with the emergence of a structure factor in the scattering. When modeling the data using a simple hard-sphere structure factor was used, the sphere radius was found to be on the order of  $60 \text{ \AA}$ , approximately  $2 \times R_{g,1}$ . The  $R_g$  scaling returns to a smaller value in this region, consistent with Borisov et al's predictions that at the highest concentrations of  $R_e \approx \phi^{-1/8}$ .

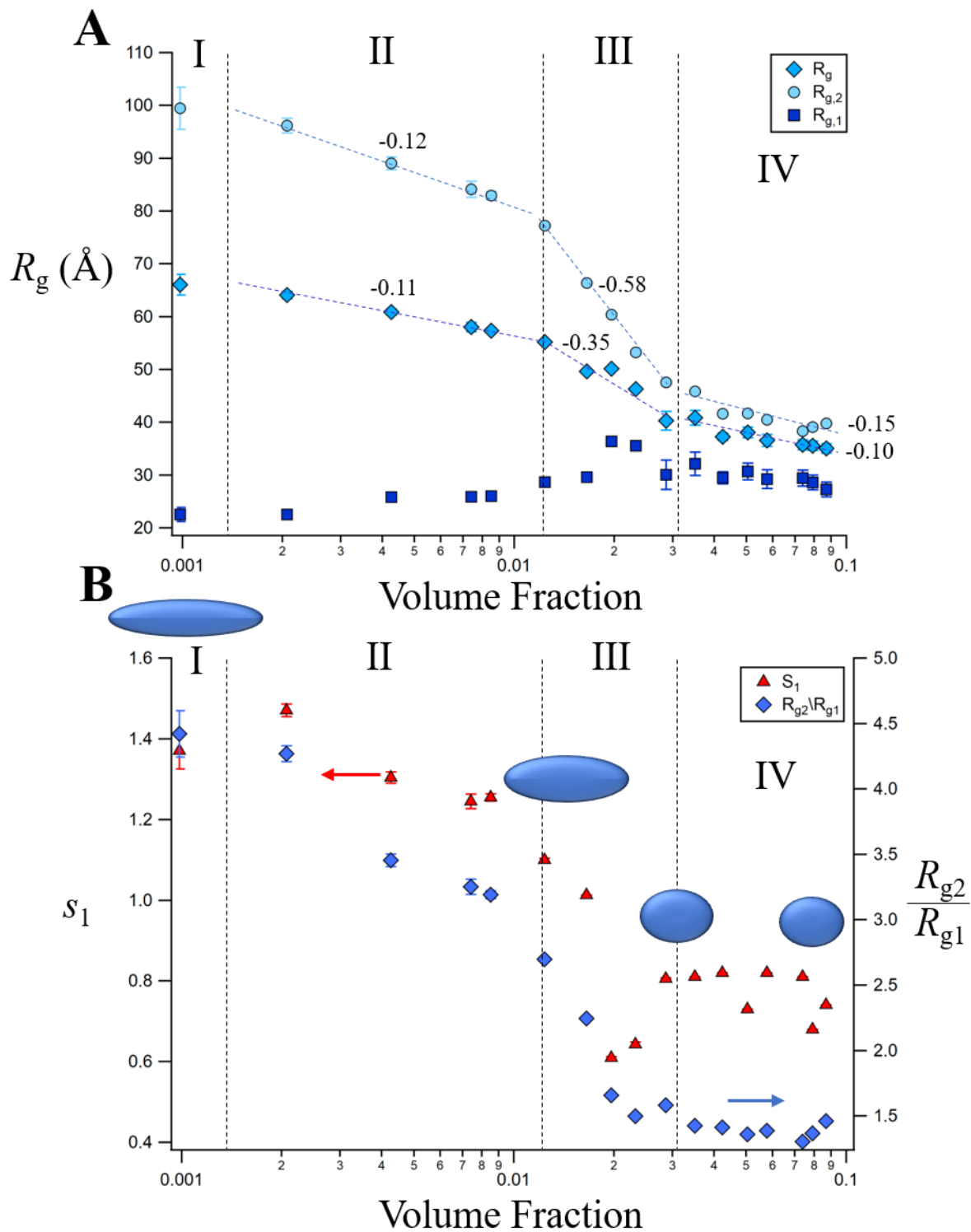


Figure 3: (A) Radius of gyration has a function of concentration for the overall  $R_g$  and both the long ( $R_{g,2}$ ) and short axis ( $R_{g,1}$ ) from fits to the data in Figure 2 using the GGP model. The four regions with different power law scalings were determined by the changes in the scaling of  $R_{g,2}$ . (B) Shape factor ( $s_1$ , left axis) and ratio of  $R_{g,2}/R_{g,1}$  (right axis). The dimensionality ( $d$ ) of the structure is related to  $s$  by  $d = 3 - s$ . Therefore, a rod-like structure will have  $s \approx 1$ . The  $R_g$  ratio provides a measure of asymmetry of the solution structure

and qualitatively tracks with  $s_1$ . The shapes at the top of the figure represent the shape of the polymer at that concentration. Error bars represent 95 % confidence intervals and are often smaller than the symbols. Detailed fit results are also provided in table 1 of the SI.

The persistence length  $l_p$  was calculated from  $R_{g,2}$  and Equation 2 as a function of concentration, the results are shown in Figure 4.  $L_c$  was calculated to be 650 Å from the contour length of the polynorbornene backbone. Similar to the trends in  $R_g$ , the  $l_p$  scaling can be broken down into four regimes. In the semi-dilute regime (II),  $l_p \sim \phi^{-0.29}$ , in the semi-concentrated regime (III)  $l_p \sim \phi^{-1.3}$ , and in the concentrated regime (IV)  $l_p \sim \phi^{-0.3}$ . In regime IV the calculated  $l_p$  was approximately 8 Å, which is on the order of the value estimated for polynorbornene (8.5 Å<sup>17</sup> or 7.1 Å<sup>50</sup>). This suggests that while the total polymer concentration is still modest, the excluded volume effects have been reduced to the point where the bottlebrush approaches melt-like conformational behavior. This is also smaller than the value estimated by Dalsin et al., who used self-consistent field theory (SCFT) coupled with experiments on diblock copolymer bottlebrush melts of varying molecular mass to extract a persistence length of  $\approx 31$  Å for norbornene brush block copolymers in the melt state.<sup>51</sup> Separately, molecular dynamics have suggested that the backbone persistence length in the melt can be approximated by the radius of the brush, which would estimate the lower bound of  $l_p \approx 20$  Å.<sup>52</sup> The approach used to extract  $l_p$  here relies on a number of approximations, and it is possible that it produces an underestimation of  $l_p$ , particularly in the concentrated regime where the scattering pattern loses some of its distinct features. This data was also fit with the flexible cylinder model, which produced unphysically low values of  $l_p$  ( $< 6$  Å) for samples in the most concentrated region. The norbornene chemistry produces more lightly grafted chains relative to the vinyl chemistry, and it is possible that this reduces the impact of the side chains on  $l_p$  in the more concentrated solutions.

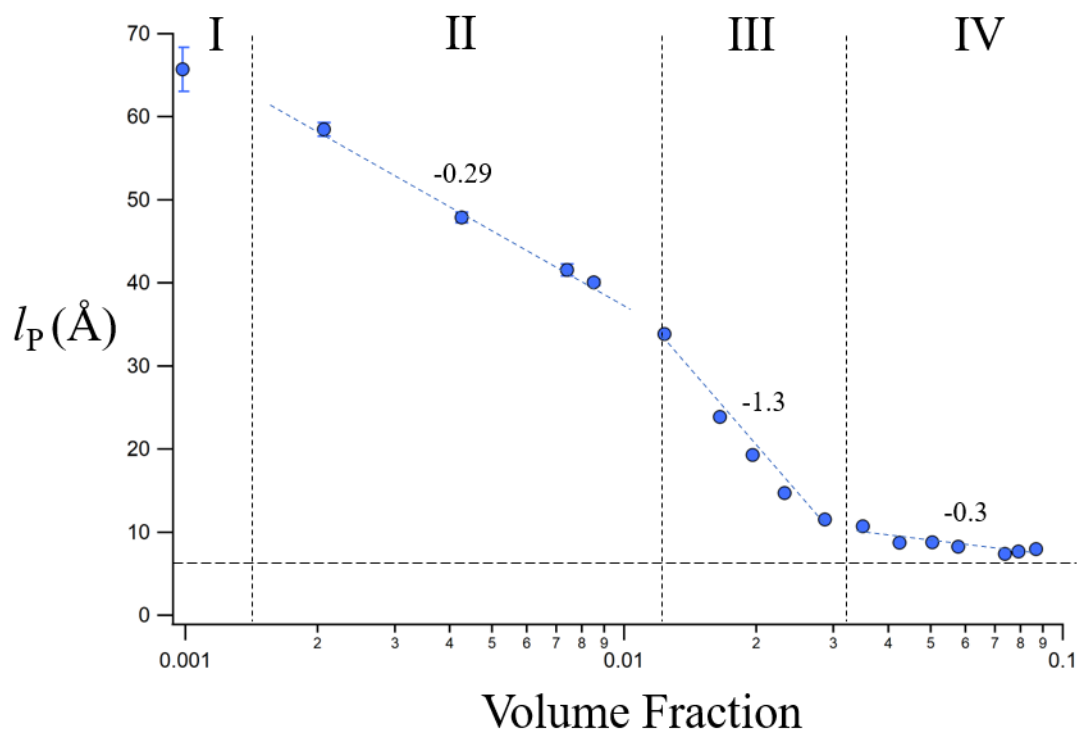


Figure 4: Log-log plot of  $l_p$  vs  $\phi$  differentiated into the four different scaling regimes as determined by the analysis of  $R_g$  scaling. The values of the scaling exponents are indicated next to the data for each regime. The dashed line indicates the estimated value for the persistence length of unfunctionalized polynorbornene,  $\sim 7.1$  Å.<sup>50</sup> Error bars represent 95 % confidence intervals and are often smaller than the symbols

## Simulation results

In addition to the experiments, complementary molecular dynamics simulations were performed to further probe the concentration dependence of bottlebrushes in solution.  $R_g$  was calculated based on the use of the path-integration algorithm ZENO, and the results are presented in Figure 5.<sup>53</sup> Initially a weak concentration dependence is observed, but above  $c/c^* \sim 0.1$  the screening of the excluded volume effects increase rapidly resulting in a rapid reduction in  $R_g$ . Eventually, in melt conditions the excluded volume interactions are screened, leading to the polymer chains having configurations effectively equivalent to random walk, *i.e.*,  $R_g \sim M_w^{1/2}$ .<sup>54</sup> This behavior shows qualitative agreement with the experimental results, where a weaker scaling dependence in the semi-dilute regime switches over to a much stronger scaling

dependence in the more concentrated regime. In the experimental results the highest concentrations result in  $l_p$  which was on the order of the linear norbornene, a result consistent with the simulation recovering a scaling for a linear random walk.

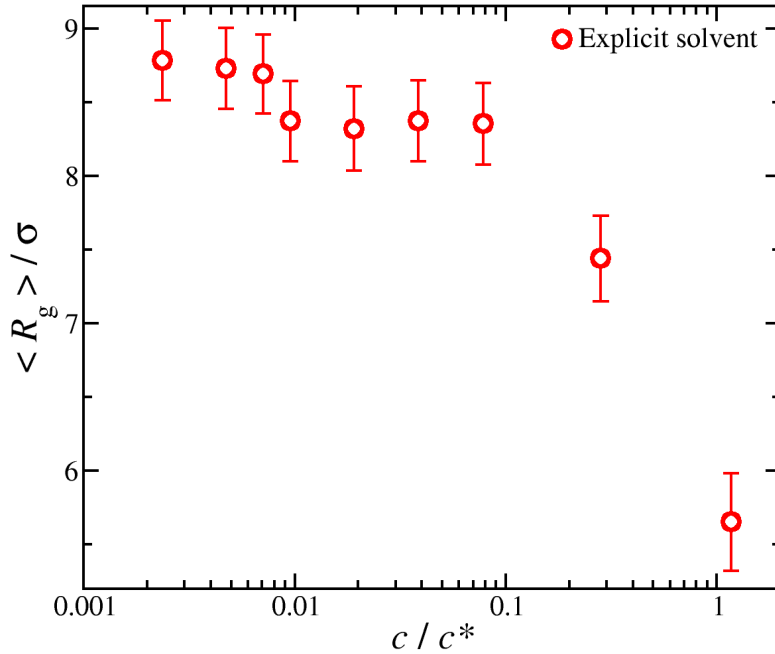


Figure 5: Average radius of gyration  $\langle R_g \rangle$  of bottlebrush polymers as a function of the polymer concentration normalized by the overlap concentration,  $c / c^*$ , where  $c^*$  is the overlap concentration. The lowest concentration simulated represents a single bottlebrush in the box, while the highest concentration simulated approaches the melt concentration. The error bars correspond to one standard deviation.

This analysis can be taken a step further by quantifying the molecular shape through the eigenvalues of the radius of gyration tensor  $S_p$ , as shown in Equation 3. These eigenvalues are denoted below by  $\lambda_1$ ,  $\lambda_2$ , and  $\lambda_3$  and are related to  $R_g^2$  as follows (Tr represents the trace operation):

$$\text{Tr } S_p = \langle R_g^2 \rangle = \langle \lambda_1 \rangle + \langle \lambda_2 \rangle + \langle \lambda_3 \rangle \quad (3)$$

where  $\lambda_1 \leq \lambda_2 \leq \lambda_3$  and the brackets  $\langle \dots \rangle$  represent time averages. The eigenvalue data are organized by comparing the two larger eigenvalues with respect to the smallest one. A sphere has  $\langle \lambda_3 \rangle / \langle \lambda_1 \rangle = \langle \lambda_2 \rangle / \langle \lambda_1 \rangle = 1$ , and an infinitely long, thin rod has  $\langle \lambda_3 \rangle / \langle \lambda_1 \rangle \rightarrow \infty$  and finite  $\langle \lambda_2 \rangle / \langle \lambda_1 \rangle$ . The ratio  $\langle \lambda_3 \rangle / \langle \lambda_1 \rangle$  characterizes the asymmetry an ellipsoidal or cylinder like molecule such as the bottlebrush and the values

for this ratio as a function of concentration are shown in Figure 6. We find that  $\langle \lambda_3 \rangle / \langle \lambda_1 \rangle$  exhibits approximately the same trends with polymer concentration as with  $R_g$  (and  $l_p^*$  as will be discussed later)., Much like the experimental results this trend shows that the change in the molecular size is accompanied by a shift towards a much more symmetric structure. The ratio  $\langle \lambda_2 \rangle / \langle \lambda_1 \rangle$  remains approximately at the same level for all polymer concentrations explored in our study. This means that the bottlebrush polymers shrink in size along the longest principal axis and explains the similarities between  $\langle \lambda_3 \rangle / \langle \lambda_1 \rangle$ ,  $R_g$ , and the persistence length as a function of the polymer concentration.

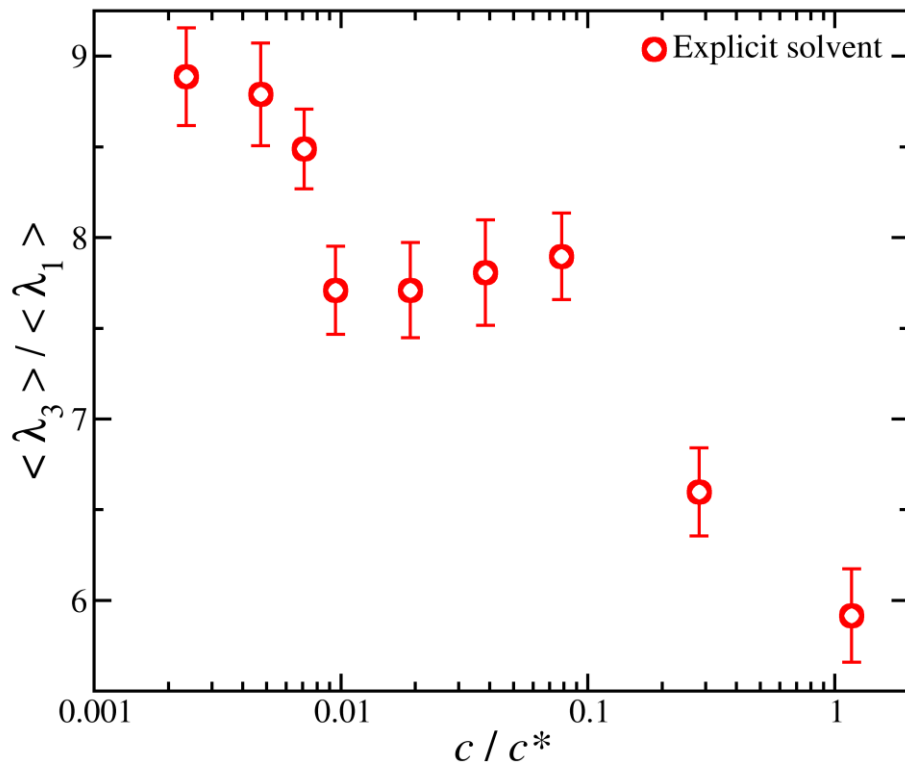


Figure 6: Ratio of the radius of gyration eigenvalues  $\langle \lambda_3 \rangle / \langle \lambda_1 \rangle$  as a function of the polymer concentration  $c$  normalized by the polymer overlap concentration,  $c^*$ .

The persistent length of macromolecules typically is calculated in simulations by the decay of the directional correlation of two segments of a macromolecule with the increase of the chain length separating them. However, there are different types of polymer flexibility.<sup>55</sup> If the polymer follows Gaussian statistics,

then the directional correlations will diminish exponentially. Thus,  $l_p$  can be obtained since the mean cosine between two segments separated by a distance  $sl_b$  along the chain can be written according to Equation 4:

$$\langle \cos \Theta(s) \rangle = \frac{\langle \vec{a}_i \cdot \vec{a}_j \rangle}{l_b^2} = e^{-sl_b l_p} \quad (4)$$

where  $\vec{a}_i$  is the bond vector along the chain,  $s = |i - j|$ , and  $l_b$  is the bond length between adjacent segments. However, it has been argued that in dense melts and in  $\theta$ -solvent conditions  $\langle \cos \Theta(s) \rangle$  scales with a power law instead of an exponential function (Equation 5),<sup>56-58</sup>

$$\langle \cos \Theta(s) \rangle = s^{-3/2} \quad \text{for } s^* < s \ll N_b \quad (5)$$

where  $s^*$  is a crossover index  $s^* \propto l_p/l_b$  between the exponential and the power law regimes. However, it becomes challenging to disentangle the crossover between the two regimes. Alternative definitions for persistence length have been proposed; however, no consensus currently exists. For in-depth discussion of different definitions, see the work by Hsu and coworkers.<sup>27</sup>

Here, we utilize the integral definition of persistent length, shown in Equation 6.<sup>59</sup> While this definition also exhibits variation with the backbone length, becoming independent for long backbones, its attractive feature is that it can consistently applied at different conditions and molecular structures, thus avoiding shortcomings arising from fitting exponential decay of the bond orientation correlations. For the molecular parameters chosen for this molecular study, we find that  $l_p^*$  exhibits significant variation with  $c$ . The basic trends as presented in Fig. 7 is that  $l_p^*$  exhibits a progressive decrease with increase of  $c$ , which is consistent with our experimental observations, compare Figs. 4 and 7. Consistent with the behavior of  $R_g$ , we also observe a deviation between the implicit and explicit solvent case, where the implicit solvent exhibits a plateau at low  $c$  and the explicit solvent shows a gradual change with  $c$ .

$$l_p^* = l_b \sum_{s=1}^{N_b} \langle \cos \Theta(s) \rangle \approx l_b \int_0^{N_b} \langle \cos \Theta(s) \rangle ds \quad (6)$$

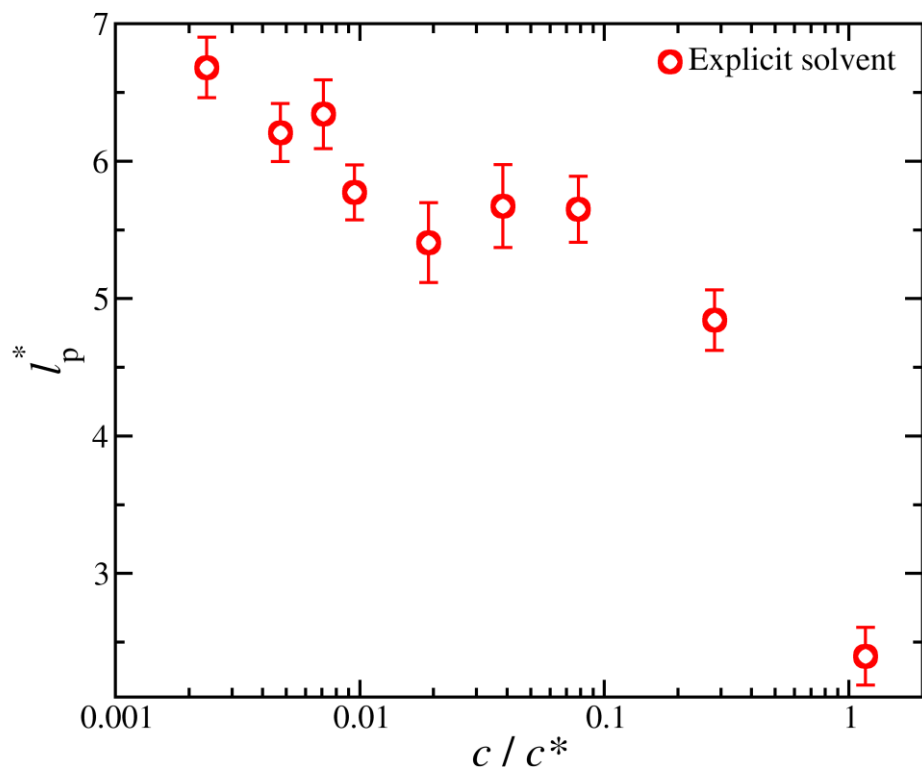


Figure 7: Persistent length of the backbone of an isolated flexible bottlebrush polymer as a function of polymer concentration normalized by the overlap polymer concentration. This was calculated through the integral definition of the persistence length shown in Equation 6.

## Conclusions

The conformations of bottlebrush polymers are highly sensitive to solution concentration. In this study the concentration dependence of the size and symmetry of a polynorbornene-based bottlebrush polymer in a good solvent was examined. Low concentrations show size-scaling behavior that matches linear chains and star polymers, but as the concentration continues to increase the scaling exponents increase sharply. The scaling exponent in the concentrated region deviates from existing predictions, suggesting that it may be necessary to consider additional contributions (such as backbone-solvent or enthalpic interactions between the backbone and sidechain) to fully understand this system. Eventually a structure factor emerges in the scattering and this combined with the estimated persistence length, suggest that the chains show features of a melt-like behavior even at relatively low volume fractions. Simulations

show qualitatively similar behavior, with simulations in explicit solvent showing a gradual change in conformation with concentration in the semi-dilute regime, followed by a more rapid change approaching the melt state. In the future, it will be worthwhile to explore if and how parameters such as backbone or side chain length impact the concentration scaling, as there is a rich space available to explore for this class of systems.

## Acknowledgements

This work benefited from the use of the SasView application, originally developed under NSF award DMR-0520547. SasView contains code developed with funding from the European Union's Horizon 2020 research and innovation programme under the SINE2020 project, grant agreement No 654000. A.B.B. acknowledges support from the National Research Council Research Associateship Program. The authors acknowledge the nSoft consortium for providing access to the NGB 10m SANS instrument.

## Supporting Information

GGP Model details, fit results and uncertainties.

## References

- (1) Fredrickson, G. H. Surfactant-Induced Lyotropic Behavior of Flexible Polymer Solutions. *Macromolecules* **1993**, *26* (11), 2825–2831. <https://doi.org/10.1021/ma00063a029>.
- (2) Beers, K. L.; Gaynor, S. G.; Matyjaszewski, K.; Sheiko, S. S.; Möller, M. The Synthesis of Densely Grafted Copolymers by Atom Transfer Radical Polymerization. *Macromolecules* **1998**, *31* (26), 9413–9415. <https://doi.org/10.1021/ma981402i>.
- (3) Runge, M. B.; Bowden, N. B. Synthesis of High Molecular Weight Comb Block Copolymers and Their Assembly into Ordered Morphologies in the Solid State. *J. Am. Chem. Soc.* **2007**, *129* (34), 10551–10560. <https://doi.org/10.1021/ja072929q>.
- (4) Xia, Y.; Olsen, B. D.; Kornfield, J. A.; Grubbs, R. H. Efficient Synthesis of Narrowly Dispersed Brush Copolymers and Study of Their Assemblies: The Importance of Side Chain Arrangement. *J. Am. Chem. Soc.* **2009**, *131* (51), 18525–18532. <https://doi.org/10.1021/ja908379q>.
- (5) Lin, T.-P.; Chang, A. B.; Luo, S.-X.; Chen, H.-Y.; Lee, B.; Grubbs, R. H. Effects of Grafting Density on Block Polymer Self-Assembly: From Linear to Bottlebrush. *ACS Nano* **2017**. <https://doi.org/10.1021/acsnano.7b06664>.
- (6) Hernandez-Garcia, A.; Werten, M. W. T.; Stuart, M. C.; de Wolf, F. A.; de Vries, R. Coating of Single DNA Molecules by Genetically Engineered Protein Diblock Copolymers. *Small* **2012**, *8* (22), 3491–3501. <https://doi.org/10.1002/sml.201200939>.
- (7) Macfarlane, R. J.; Kim, B.; Lee, B.; Weitekamp, R. A.; Bates, C. M.; Lee, S. F.; Chang, A. B.; Delaney, K. T.; Fredrickson, G. H.; Atwater, H. A.; Grubbs, R. H. Improving Brush Polymer

- Infrared One-Dimensional Photonic Crystals via Linear Polymer Additives. *J. Am. Chem. Soc.* **2014**, *136* (50), 17374–17377. <https://doi.org/10.1021/ja5093562>.
- (8) Sveinbjörnsson, B. R.; Weitekamp, R. A.; Miyake, G. M.; Xia, Y.; Atwater, H. A.; Grubbs, R. H. Rapid Self-Assembly of Brush Block Copolymers to Photonic Crystals. *Proc. Natl. Acad. Sci.* **2012**, *109* (36), 14332–14336.
  - (9) Xu, H.; Sun, F. C.; Shirvanyants, D. G.; Rubinstein, M.; Shabratov, D.; Beers, K. L.; Matyjaszewski, K.; Sheiko, S. S. Molecular Pressure Sensors. *Adv. Mater.* **2007**, *19* (19), 2930–2934. <https://doi.org/10.1002/adma.200602376>.
  - (10) Arrington, K. J.; Radzinski, S. C.; Drummey, K. J.; Long, T. E.; Matson, J. B. Reversibly Cross-Linkable Bottlebrush Polymers as Pressure-Sensitive Adhesives. *ACS Appl. Mater. Interfaces* **2018**, *10* (31), 26662–26668. <https://doi.org/10.1021/acsami.8b08480>.
  - (11) Vatankhah-Varnosfaderani, M.; Keith, A. N.; Cong, Y.; Liang, H.; Rosenthal, M.; Sztucki, M.; Clair, C.; Magonov, S.; Ivanov, D. A.; Dobrynin, A. V.; Sheiko, S. S. Chameleon-like Elastomers with Molecularly Encoded Strain-Adaptive Stiffening and Coloration. *Science* **2018**, *359*, 1509–1513.
  - (12) Hsu, H.-P.; Paul, W.; Rathgeber, S.; Binder, K. Characteristic Length Scales and Radial Monomer Density Profiles of Molecular Bottle-Brushes: Simulation and Experiment. *Macromolecules* **2010**, *43* (3), 1592–1601. <https://doi.org/10.1021/ma902101n>.
  - (13) Chremos, A.; Douglas, J. F. A Comparative Study of Thermodynamic, Conformational, and Structural Properties of Bottlebrush with Star and Ring Polymer Melts. *J. Chem. Phys.* **2018**, *149* (4), 044904. <https://doi.org/10.1063/1.5034794>.
  - (14) Pesek, S. L.; Li, X.; Hammouda, B.; Hong, K.; Verduzco, R. Small-Angle Neutron Scattering Analysis of Bottlebrush Polymers Prepared via Grafting-Through Polymerization. *Macromolecules* **2013**, *46* (17), 6998–7005. <https://doi.org/10.1021/ma401246b>.
  - (15) Rathgeber, S.; Pakula, T.; Wilk, A.; Matyjaszewski, K.; Beers, K. L. On the Shape of Bottle-Brush Macromolecules: Systematic Variation of Architectural Parameters. *J. Chem. Phys.* **2005**, *122* (12), 124904. <https://doi.org/10.1063/1.1860531>.
  - (16) Zhang, B.; Gröhn, F.; Pedersen, J. S.; Fischer, K.; Schmidt, M. Conformation of Cylindrical Brushes in Solution: Effect of Side Chain Length. *Macromolecules* **2006**, *39* (24), 8440–8450. <https://doi.org/10.1021/ma0613178>.
  - (17) Liang, H.; Cao, Z.; Wang, Z.; Sheiko, S. S.; Dobrynin, A. V. Combs and Bottlebrushes in a Melt. *Macromolecules* **2017**, *50* (8), 3430–3437. <https://doi.org/10.1021/acs.macromol.7b00364>.
  - (18) Bolisetty, S.; Airaud, C.; Xu, Y.; Müller, A. H. E.; Harnau, L.; Rosenfeldt, S.; Lindner, P.; Ballauff, M. Softening of the Stiffness of Bottle-Brush Polymers by Mutual Interaction. *Phys. Rev. E* **2007**, *75* (4). <https://doi.org/10.1103/PhysRevE.75.040803>.
  - (19) Storm, I. M.; Kornreich, M.; Voets, I. K.; Beck, R.; de Vries, R.; Cohen Stuart, M. A.; Leermakers, F. A. M. Loss of Bottlebrush Stiffness Due to Free Polymers. *Soft Matter* **2016**, *12* (38), 8004–8014. <https://doi.org/10.1039/C6SM01227B>.
  - (20) Rathgeber, S.; Pakula, T.; Wilk, A.; Matyjaszewski, K.; Lee, H.; Beers, K. L. Bottle-Brush Macromolecules in Solution: Comparison between Results Obtained from Scattering Experiments and Computer Simulations. *Polymer* **2006**, *47* (20), 7318–7327. <https://doi.org/10.1016/j.polymer.2006.06.010>.
  - (21) Paturej, J.; Kreer, T. Hierarchical Excluded Volume Screening in Solutions of Bottlebrush Polymers. *Soft Matter* **2017**, *13* (45), 8534–8541. <https://doi.org/10.1039/C7SM01968H>.
  - (22) Birshtein, T. M.; Borisov, O. V.; Zhulina, Ye. B.; Khokhlov, A. R.; Yurasova, T. A. Conformations of Comb-like Macromolecules. *Polym. Sci. USSR* **1987**, *29* (6), 1293–1300. [https://doi.org/10.1016/0032-3950\(87\)90374-1](https://doi.org/10.1016/0032-3950(87)90374-1).
  - (23) Borisov, O. V.; Birshtein, T. M.; Zhulina, Ye. B. The Temperature-Concentration Diagram of State for Solutions of Comb-like Macromolecules. *Polym. Sci. USSR* **1987**, *29* (7), 1552–1559. [https://doi.org/10.1016/0032-3950\(87\)90416-3](https://doi.org/10.1016/0032-3950(87)90416-3).

- (24) Dutta, S.; Wade, M. A.; Walsh, D. J.; Guironnet, D.; Rogers, S. A.; Sing, C. E. Dilute Solution Structure of Bottlebrush Polymers. *Soft Matter* **2019**. <https://doi.org/10.1039/C9SM00033J>.
- (25) Levi, A. E.; Lequieu, J.; Horne, J. D.; Bates, M. W.; Ren, J. M.; Delaney, K. T.; Fredrickson, G. H.; Bates, C. M. Miktoarm Stars via Grafting-Through Copolymerization: Self-Assembly and the Star-to-Bottlebrush Transition. *Macromolecules* **2019**, *52* (4), 1794–1802. <https://doi.org/10.1021/acs.macromol.8b02321>.
- (26) Kikuchi, M.; Lien, L. T. N.; Narumi, A.; Jinbo, Y.; Izumi, Y.; Nagai, K.; Kawaguchi, S. Conformational Properties of Cylindrical Rod Brushes Consisting of a Polystyrene Main Chain and Poly(*n*-Hexyl Isocyanate) Side Chains. *Macromolecules* **2008**, *41* (17), 6564–6572. <https://doi.org/10.1021/ma800951d>.
- (27) Hsu, H.-P.; Paul, W.; Binder, K. Standard Definitions of Persistence Length Do Not Describe the Local “Intrinsic” Stiffness of Real Polymer Chains. *Macromolecules* **2010**, *43* (6), 3094–3102. <https://doi.org/10.1021/ma902715e>.
- (28) Hsu, H.-P.; Paul, W.; Binder, K. Understanding the Multiple Length Scales Describing the Structure of Bottle-Brush Polymers by Monte Carlo Simulation Methods. *Macromol. Theory Simul.* **2011**, *20* (7), 510–525. <https://doi.org/10.1002/mats.201000092>.
- (29) Pesek, S. L.; Xiang, Q.; Hammouda, B.; Verduzco, R. Small-Angle Neutron Scattering Analysis of Bottlebrush Backbone and Side Chain Flexibility. *J. Polym. Sci. Part B Polym. Phys.* **2016**. <https://doi.org/10.1002/polb.24251>.
- (30) Ahn, S.; Carrillo, J.-M. Y.; Han, Y.; Kim, T.-H.; Uhrig, D.; Pickel, D. L.; Hong, K.; Kilbey, S. M.; Sumpter, B. G.; Smith, G. S.; Do, C. Structural Evolution of Polylactide Molecular Bottlebrushes: Kinetics Study by Size Exclusion Chromatography, Small Angle Neutron Scattering, and Simulations. *ACS Macro Lett.* **2014**, *3* (9), 862–866. <https://doi.org/10.1021/mz5003454>.
- (31) Li, X.; ShamsiJazeyi, H.; Pesek, S. L.; Agrawal, A.; Hammouda, B.; Verduzco, R. Thermoresponsive PNIPAAm Bottlebrush Polymers with Tailored Side-Chain Length and End-Group Structure. *Soft Matter* **2014**, *10* (12), 2008. <https://doi.org/10.1039/c3sm52614c>.
- (32) Aviv, Y.; Altay, E.; Fink, L.; Raviv, U.; Rzayev, J.; Shenhar, R. Quasi-Two-Dimensional Assembly of Bottlebrush Block Copolymers with Nanoparticles in Ultrathin Films: Combined Effect of Graft Asymmetry and Nanoparticle Size. *Macromolecules* **2019**, *52* (1), 196–207. <https://doi.org/10.1021/acs.macromol.8b01988>.
- (33) Willner, L.; Jucknischke, O.; Richter, D.; Roovers, J.; Zhou, L.-L.; Toporowski, P. M.; Fetters, L. J.; Huang, J. S.; Lin, M. Y.; Hadjichristidis, N. Structural Investigation of Star Polymers in Solution by Small-Angle Neutron Scattering. *Macromolecules* **1994**, *27* (14), 3821–3829. <https://doi.org/10.1021/ma00092a022>.
- (34) Daoud, M.; Cotton, J. P. Star Shaped Polymers : A Model for the Conformation and Its Concentration Dependence. *J. Phys.* **1982**, *43* (3), 531–538. <https://doi.org/10.1051/jphys:01982004303053100>.
- (35) Ying, Qicong.; Chu, Benjamin. Overlap Concentration of Macromolecules in Solution. *Macromolecules* **1987**, *20* (2), 362–366. <https://doi.org/10.1021/ma00168a023>.
- (36) Hammouda, B. A New Guinier–Porod Model. *J. Appl. Crystallogr.* **2010**, *43* (4), 716–719. <https://doi.org/10.1107/S0021889810015773>.
- (37) Sunday, D. F.; Martin, T. B.; Chang, A. B.; Burns, A. B.; Grubbs, R. H. Addressing the Challenges of Modeling the Scattering from Bottlebrush Polymers in Solution. *J. Polym. Sci.* **2020**, *pol.20190289*. <https://doi.org/10.1002/pol.20190289>.
- (38) Zhang, Z.; Carrillo, J.-M. Y.; Ahn, S.; Wu, B.; Hong, K.; Smith, G. S.; Do, C. Atomistic Structure of Bottlebrush Polymers: Simulations and Neutron Scattering Studies. *Macromolecules* **2014**, *47* (16), 5808–5814. <https://doi.org/10.1021/ma500613c>.
- (39) Dutta, S.; Pan, T.; Sing, C. E. Bridging Simulation Length Scales of Bottlebrush Polymers Using a Wormlike Cylinder Model. *Macromolecules* **2019**, *acs.macromol.9b00363*. <https://doi.org/10.1021/acs.macromol.9b00363>.

- (40) Benoit, H.; Doty, P. Light Scattering from Non-Gaussian Chains. *J. Phys. Chem.* **1953**, *57* (9), 958–963. <https://doi.org/10.1021/j150510a025>.
- (41) Grest, G. S.; Kremer, K.; Milner, S. T.; Witten, T. A. Relaxation of Self-Entangled Many-Arm Star Polymers. *Macromolecules* **1989**, *22* (4), 1904–1910. <https://doi.org/10.1021/ma00194a065>.
- (42) Chremos, A.; Camp, P. J.; Glynos, E.; Koutsos, V. Adsorption of Star Polymers: Computer Simulations. *Soft Matter* **2010**, *6* (7), 1483. <https://doi.org/10.1039/b922988d>.
- (43) Saunders, M. G.; Voth, G. A. Coarse-Graining Methods for Computational Biology. *Annu. Rev. Biophys.* **2013**, *42* (1), 73–93. <https://doi.org/10.1146/annurev-biophys-083012-130348>.
- (44) Chaimovich, A.; Shell, M. S. Coarse-Graining Errors and Numerical Optimization Using a Relative Entropy Framework. *J. Chem. Phys.* **2011**, *134* (9), 094112. <https://doi.org/10.1063/1.3557038>.
- (45) Bates, C. M.; Chang, A. B.; Momčilović, N.; Jones, S. C.; Grubbs, R. H. ABA Triblock Brush Polymers: Synthesis, Self-Assembly, Conductivity, and Rheological Properties. *Macromolecules* **2015**, *48* (14), 4967–4973. <https://doi.org/10.1021/acs.macromol.5b00880>.
- (46) Certain Commercial Equipment, Instruments, or Materials Are Identified in This Paper in Order to Specify the Experimental Procedure Adequately. Such Identification Is Not Intended to Imply Recommendation or Endorsement by the National Institute of Standards and Technology, nor Is It Intended to Imply That the Materials or Equipment Identified Are Necessarily the Best Available for the Purpose.
- (47) Vrugt, J. A.; Ter Braak, C. J. F. DREAM<Sub>(D)</Sub>: An Adaptive Markov Chain Monte Carlo Simulation Algorithm to Solve Discrete, Noncontinuous, and Combinatorial Posterior Parameter Estimation Problems. *Hydrol. Earth Syst. Sci.* **2011**, *15* (12), 3701–3713. <https://doi.org/10.5194/hess-15-3701-2011>.
- (48) Chremos, A.; Nikoubashman, A.; Panagiotopoulos, A. Z. Flory-Huggins Parameter  $\chi$ , from Binary Mixtures of Lennard-Jones Particles to Block Copolymer Melts. *J. Chem. Phys.* **2014**, *140* (5), 054909. <https://doi.org/10.1063/1.4863331>.
- (49) Plimpton, S. Fast Parallel Algorithms for Short-Range Molecular Dynamics. *J. Comput. Phys.* **1995**, *117*, 1–19.
- (50) Liu, C.; Kubo, K.; Wang, E.; Han, K.-S.; Yang, F.; Chen, G.; Escobedo, F. A.; Coates, G. W.; Chen, P. Single Polymer Growth Dynamics. *Science* **2017**, *358* (6361), 352–355. <https://doi.org/10.1126/science.aan6837>.
- (51) Dalsin, S. J.; Rions-Maehren, T. G.; Beam, M. D.; Bates, F. S.; Hillmyer, M. A.; Matsen, M. W. Bottlebrush Block Polymers: Quantitative Theory and Experiments. *ACS Nano* **2015**, *9* (12), 12233–12245. <https://doi.org/10.1021/acsnano.5b05473>.
- (52) Cao, Z.; Carrillo, J.-M. Y.; Sheiko, S. S.; Dobrynin, A. V. Computer Simulations of Bottle Brushes: From Melts to Soft Networks. *Macromolecules* **2015**, *48* (14), 5006–5015. <https://doi.org/10.1021/acs.macromol.5b00682>.
- (53) Juba, D.; Audus, D. J.; Mascagni, M.; Douglas, J. F.; Keyrouz, W. ZENO: Software for Calculating Hydrodynamic, Electrical, and Shape Properties of Polymer and Particle Suspensions. *J. Res. Natl. Inst. Stand. Technol.* **2017**, *122*, 20. <https://doi.org/10.6028/jres.122.020>.
- (54) Flory, P. J. *Statistical Mechanics of Chain Molecules*; Interscience: New York, NY, 1969.
- (55) Grosberg, A. Y.; Khokhlov, A. R. *Statistical Physics of Macromolecules*; AIP: New York, NY, 1994.
- (56) Shirvanyants, D.; Panyukov, S.; Liao, Q.; Rubinstein, M. Long-Range Correlations in a Polymer Chain Due to Its Connectivity. *Macromolecules* **2008**, *41* (4), 1475–1485. <https://doi.org/10.1021/ma071443r>.
- (57) Wittmer, J. P.; Beckrich, P.; Meyer, H.; Cavallo, A.; Johner, A.; Baschnagel, J. Intramolecular Long-Range Correlations in Polymer Melts: The Segmental Size Distribution and Its Moments. *Phys. Rev. E* **2007**, *76* (1), 011803. <https://doi.org/10.1103/PhysRevE.76.011803>.

- (58) Wittmer, J. P.; Meyer, H.; Baschnagel, J.; Johner, A.; Obukhov, S.; Mattioni, L.; Müller, M.; Semenov, A. N. Long Range Bond-Bond Correlations in Dense Polymer Solutions. *Phys. Rev. Lett.* **2004**, *93* (14), 147801. <https://doi.org/10.1103/PhysRevLett.93.147801>.
- (59) Hsu, H.-P.; Binder, K.; Paul, W. How to Define Variation of Physical Properties Normal to an Undulating One-Dimensional Object. *Phys. Rev. Lett.* **2009**, *103* (19), 198301. <https://doi.org/10.1103/PhysRevLett.103.198301>.

# The Concentration Dependence of the Size and Symmetry of a Bottlebrush Polymer in a Good Solvent

Daniel F. Sunday<sup>1\*</sup>, Alexandros Chremos,<sup>1\*</sup> Tyler B. Martin<sup>1</sup>, Alice B. Chang<sup>2</sup>, Adam B. Burns<sup>1</sup>, Robert H. Grubbs<sup>2</sup>

1. Materials Science and Engineering Division, National Institute of Standards and Technology, Gaithersburg, MD 20899, United States
2. Division of Chemistry and Chemical Engineering, California Institute of Technology, Pasadena, CA 91125, United States

\* [Daniel.Sunday@nist.gov](mailto:Daniel.Sunday@nist.gov), [Alexandros.Chremos@nist.gov](mailto:Alexandros.Chremos@nist.gov)

## Supplemental Information

The general Guiner-Porod (GGP) model is described by Equations 1-3.<sup>1</sup> This model describes the scattering by using Guinier regions interconnected by power law regimes. Crossover points ( $Q_1$ ,  $Q_2$ ) and scaling factors ( $G_1, G_2$ ) are calculated to ensure self-consistency in the transition between different regions. The model uses shape factors ( $s_1, s_2$ ) to describe the approximate shape of the scattering features, where 0 represents a sphere, 1 represents a cylinder or rod, and 2 represents lamellae. A background and intensity scaling term were also included in the model. The implementation of the general Guinier-Porod model in Sasview is available in the Sasview marketplace (<http://marketplace.sasview.org/>), with the model name “2 Layer General Guinier Porod”. The hard sphere structure factor was used where appropriate and its implementation is described in the sasview documentation.

$$I(Q) = \frac{G_2}{Q^{s_2}} \exp\left(-\frac{Q^2 R_{g,2}^2}{3-s_2}\right) \text{ for } Q \leq Q_2 \quad (1)$$

$$I(Q) = \frac{G_1}{Q^{s_1}} \exp\left(-\frac{Q^2 R_{g,1}^2}{3-s_1}\right) \text{ for } Q_2 \leq Q \leq Q_1 \quad (2)$$

$$I(Q) = \frac{D}{Q^d} \text{ for } Q \geq Q_1 \quad (3)$$

Table 1: Fit Results to GGP model (Figures 3 and 4). Uncertainties represent 95% confidence intervals as evaluated by the Monte-Carlo Markov Chain analysis performed by the Dream algorithm in Sasview.

<b>Volume Fraction</b>	$R_{g,2}$ (Å)	$R_{g,1}$ (Å)	$R_g$	$s_1$	$s_2$	$l_p$ (Å)
0.0870	39.8 ± 0.1	27.3 ± 0.1	35.0 ± 0.9	0.74 ± 0.13	0	7.9 ± 0.1
0.0792	39.0 ± 0.2	28.6 ± 0.1	35.5 ± 0.9	0.68 ± 0.15	0	7.7 ± 0.1
0.0739	38.3 ± 0.1	29.4 ± 0.1	35.8 ± 1.0	0.98 ± 0.18	0	7.4 ± 0.1
0.0578	40.5 ± 0.1	29.2 ± 0.1	36.6 ± 1.1	0.82 ± 0.12	0	8.2 ± 0.1
0.0504	41.7 ± 0.1	30.7 ± 0.1	38.0 ± 1.0	0.73 ± 0.15	0	8.8 ± 0.1
0.0424	41.6 ± 0.2	29.5 ± 0.1	37.2 ± 0.7	0.88 ± 0.16	0	8.7 ± 0.1
0.0350	45.8 ± 0.1	32.2 ± 0.1	40.8 ± 1.4	0.9 ± 0.18	0	10.7 ± 0.1
0.0287	47.5 ± 0.2	30.0 ± 0.1	40.3 ± 1.7	0.8 ± 0.33	0	11.5 ± 0.1
0.0232	53.2 ± 0.4	35.5 ± 0.1	46.3 ± 0.2	0.64 ± 0.08	0	14.7 ± 0.1
0.0196	60.3 ± 0.3	36.4 ± 0.1	50.1 ± 0.2	0.61 ± 0.05	0	19.3 ± 0.1
0.0165	66.4 ± 0.1	29.5 ± 0.1	49.6 ± 0.2	1.01 ± 0.08	0	23.9 ± 0.1
0.0124	77.2 ± 0.3	28.6 ± 0.1	55.2 ± 0.2	1.1 ± 0.09	0	33.8 ± 0.2
0.0085	82.9 ± 0.8	26.0 ± 0.1	57.3 ± 0.4	1.25 ± 0.10	0.1 ± 0.01	40 ± 0.4
0.0074	84.1 ± 1.5	25.9 ± 0.1	58.0 ± 0.9	1.24 ± 0.11	0.2 ± 0.02	41.6 ± 0.8
0.0043	89.0 ± 1.2	25.8 ± 0.1	60.8 ± 0.6	1.3 ± 0.03	0.1 ± 0.01	47.9 ± 0.7
0.0021	96.2 ± 1.4	22.5 ± 0.1	64.1 ± 0.7	1.47 ± 0.04	0.1 ± 0.02	58.5 ± 0.8
0.0010	99.5 ± 4.0	22.5 ± 0.1	66.0 ± 2	1.37 ± 0.06	0.1 ± 0.05	65.7 ± 2.7

## References

- (1) Hammouda, B. A New Guinier–Porod Model. *J. Appl. Crystallogr.* **2010**, *43* (4), 716–719.  
<https://doi.org/10.1107/S0021889810015773>.